ACS APPLIED MATERIALS & INTERFACES

Research Article

www.acsami.org

Superhydrophobic Stability of Nanotube Array Surfaces under Impact and Static Forces

Lin Zhu,[†] Pan Shi,[†] Jian Xue,[†] Yuanyi Wang,[†] Qingmin Chen,[†] Jianfu Ding,[‡] and Qingjun Wang*[,†]

[†]Polymer Science and Engineering Department, School of Chemistry and Chemical Engineering, State Key Laboratory of Coordination Chemistry, Nanjing University, Nanjing, Jiangsu 210093, China

[‡]Security and Disruptive Technologies, National Research Council Canada, 1200 Montreal Road, Ottawa, Ontario K1A 0R6, Canada

Supporting Information

ABSTRACT: The surfaces of nanotube arrays were coated with poly(methyl methacrylate) (PMMA) using an imprinting method with an anodized alumina membrane as the template. The prepared nanotube array surfaces then either remained untreated or were coated with $NH_2(CH_2)_3Si(OCH_3)_3$(PDNS) or $CF_3(CF_2)_7CH_2CH_2Si(OC_2H_5)_3$ (PFO). Thus, nanotube arrays with three different surfaces, PDNS, PMMA (without coating), and PFO, were obtained. All three surfaces (PDNS, PMMA, and PFO) exhibited superhydrophobic properties with contact angles (CA) of 155, 166, and 168°, respectively, and their intrinsic water contact angles were 30, 79, and 118°, respectively. The superhydrophobic stabilities of these three surfaces were examined under dynamic impact and static pressures in terms of the transition from the Cassie−Baxter mode to the Wenzel mode. This transition was determined by the maximum pressure (p^{max}), which is dependent on the intrinsic contact angle and the nanotube density of the surface. A p^{max} greater than 10 kPa, which is sufficiently large to maintain stable superhydrophobicity under extreme weather conditions, such as in heavy rain, was expected from the PFO surface. Interestingly, the PDNS surface, with an intrinsic CA of only 30°, also displayed superhydrophobicity, with a CA of 155°. This property was partially maintained under the dynamic impact and static pressure tests. However, under an extremely high pressure (0.5 MPa), all three surfaces transitioned from the Cassie−Baxter mode to the Wenzel mode. Furthermore, the lost superhydrophobicity could not be recovered by simply relieving the pressure. This result indicates that the best way to maintain superhydrophobicity is to increase the p^{max} of the surface to a value higher than the applied external pressure by using low surface energy materials and having high-density binary nano-/microstructures on the surface.

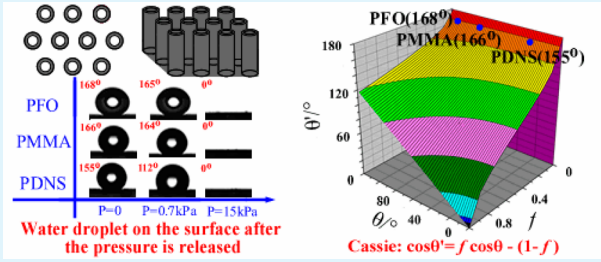

KEYWORDS: *nanotube array, superhydrophobic, energy barrier, wetting state transition, external pressure*

INTRODUCTION

The superhydrophobic phenomenon, also known as the lotus effect, has attracted considerable attention because of its numerous potential applications.[1] A superhydrophobic material generally displays a large contact angle (CA, greater than 150°) and a small slide angle (SA, less than 5°).[2] The superhydrophobicity of a surface is determined by the topological structure of the surface and its intrinsic hydrophobicity. The latter is associated with the chemical composition of the surface. A binary nano-/microsurface structure is essential for achieving superhydrophobic properties. For many applications, the stability of the obtained superhydrophobicity is very important. Many superhydrophobic surfaces (both synthetic and natural) cannot maintain their superhydrophobicity under harsh environmental conditions, such as in low temperatures and heavy rain. Several methods have been introduced to improve superhydrophobic stability by increasing the durability of surface nano-/microstructures and optimizing the chemical composition. For example, a durable aluminum surface with randomly distributed nano-/micropetals was prepared by acid etching,[3−6] a highly ordered nano-/micropillar array surface structure was made by laser ablation,[2,7−10] and a polymer surface with polyethylene nanowire arrays was fabricated by nano-injection molding.[11]

A superhydrophobic surface in contact with a water droplet forms a water−air−solid composite interface. The contact angle of the water droplet (θ') can be described by the Cassie−Baxter equation:

$$\cos\theta' = f\cos\theta - (1 - f) \quad (1)$$

where f is the fraction of the water−solid area, and θ is the intrinsic water contact angle of the substrate. This equation indicates that the contact angle $\theta'$is always larger than θ on both hydrophobic ($\theta > 90°$) and hydrophilic ($\theta < 90°$) substrates as long as the water-air interface is formed ($f < 1$). The contact angle θ'will be significantly enhanced by decreasing the water−solid contact area f. However, the Cassie−Baxter state of a water droplet on a rough hydrophilic

Received: January 13, 2014
Accepted: May 19, 2014
Published: May 29, 2014

surface is often unstable or metastable. The water droplet can enter the grooves of the nano-/microstructures on the rough surface to eliminate the water−air interface. This process will ultimately convert the surface from the Cassie−Baxter mode to the Wenzel mode. At this state, the water contact angle follows the Wenzel equation

$$\cos\theta' = r\cos\theta \tag{2}$$

where r is the surface roughness and is usually calculated as the ratio of the total area of the rough surface to its projected area. Comparing these two equations, we can see that a superhydrophobic surface is required to maintain a droplet in the Cassie−Baxter state. The stability of superhydrophobic surfaces and the transition from the Cassie−Baxter mode to the Wenzel mode have been intensively studied through experimental analyses and numerical simulations.[12−14] The energy barrier for transition from the Cassie−Baxter state to the Wenzel state on a superhydrophobic surface can be determined from the maximum pressure, p^{max}. Lobaton and Salamon derived the following equation for calculating p^{max} based on a periodic circular pillar array[15]

$$p^{max} = -\frac{\gamma L\cos\theta}{A} \tag{3}$$

where γ is the surface tension of water, A is the projected water−air interface area, and L is the sum of the perimeter of the pillars. This equation indicates that the Cassie−Baxter stability depends on the surface structure and the hydrophobicity of the substrate. On the basis of the periodic circular pillar array model with a pillar radius of R[15], we can represent the L and A values by $L = 2n\pi R$, and $A = (S - n\pi R^2)$. The latter can be rewritten as $A = n\pi R^2(1 - f)/f$ because $f = n\pi R^2/S$ under the assumption that the entire pillar is in contact with water. Here, n is the total number of pillars, and S is the total surface area. eq 3 can be rewritten as

$$p^{max} = -\frac{2\gamma f\cos\theta}{R(1 - f)} \tag{4}$$

This equation states that p^{max} will increase with the water−solid fraction (f). Therefore, although an increased f value will yield a lower superhydrophobicity according to eq 1, increasing the p^{max} value to the external pressure stabilizes the superhydrophobicity. When an external pressure exceeding p^{max} is applied to the water droplet, water can then be pushed into the grooves of the rough surface structure to transition the surface from the Cassie−Baxter state to the Wenzel state. From this equation, we can also see that a positive p^{max} value, which is essential for maintaining surface superhydrophobicity, can only be achieved for a substrate with $\theta > 90°$. Similar conclusions have been reached by other researchers.[16−20]

In contrast, a positive p^{max} value can also be obtained from a hydrophilic substrate with $\theta < 90°$ when special geometries are created on top of the pillars.[15] For example, pillars with a nail-head structure will give positive p^{max} values on a substrate with $\theta \le 90°$, which can be calculated from eq 4.

$$p^{max} = \frac{\gamma L\sin\theta}{A} \text{for } \theta \le 90° \tag{5}$$

This equation indicates that a positive p^{max} for maintaining the surface at the Cassie−Baxter mode can be created even on a hydrophilic substrate under the condition that special geometries are created on top of the pillars.

In this work, we prepared a surface covered with nanotube arrays, which was then modified by silicon coupling agents to obtain three surfaces with different hydrophobicities. The intrinsic water contact angles (θ) of the surfaces were 30, 79, and 118°. These three surfaces all showed superhydrophobicity under normal conditions. The superhydrophobic stability was examined by applying impact and static pressures on the surfaces. The stability obeyed eqs 3 and 5 for the hydrophobic and hydrophilic substrates, respectively. When the applied pressure exceeds the maximum pressure (p^{max}), the transition from the Cassie−Baxter mode to the Wenzel mode occurs, and this transition is irreversible when the external pressure is removed.

EXPERIMENTAL SECTION

Nanotube Fabrication. A porous anodic alumina (AAO) template was heated to 60 °C in a vacuum oven. A piece of PMMA (~1 g) was placed on top of the template to prevent the template from curling because of thermal expansion. The temperature was then raised to 190°C and maintained for 30 min to melt the PMMA into the pores of the template. After cooling to room temperature, the sample was soaked in a 0.5 mol/L NaOH solution until the template was dissolved completely and then rinsed with distilled water several times. The sample was stored in a vacuum desiccator prior to use.

Surface Modification. PFO($CF_3(CF_2)_7CH_2CH_2Si(OC_2H_5)_3$) and PDNS ($NH_2(CH_2)_3Si(OCH_3)_3$) coating solutions were prepared by mixing PFO (0.5 wt %) and PDNS (0.5 wt %) with a mixture of methanol (88 wt %), deionized water (10 wt %) and HCl (0.1 M, 1.5 wt %). The PMMA nanotube array sample was immersed in the coating solution and sonicated for 10 min in a bath sonicator. The sample was then removed from the solution and air dried. This process was repeated three times. The sample was then placed in a thermostat at 75 °C for 24 h to completely crosslink the PFO and PDNS coatings.

Dynamic Impact Test. The water impact process was monitored with a high-speed camera (Phantom V-710, USA) at a speed of 4000 p/s (frame per second). The entire impact process, from water droplet release at a predetermined height with zero initial velocity to impact at the surface and the approach to equilibrium, was recorded.

Mechanical Static Pressure Test. As illustrated in Figure 1, the sample was fixed on the base with the nanotube array surface facing up,

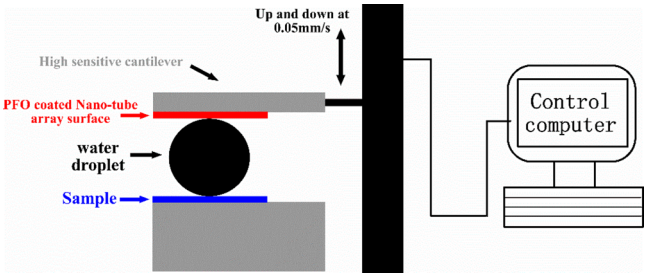

Figure 1. Diagram of the set up for the mechanical static pressure test.

and a water droplet was placed on the sample. Meanwhile, the compression unit on the cantilever was covered by a sample of PFO, with the nanotube array surface facing the droplet. The compression unit moved toward the droplet under control by a computer at a speed of 0.1 mm/s until the desired force was reached. The shape of the droplet was recorded. The compression force was then released at a low speed of 50 μm/s to minimize the disturbance of the droplet. The droplet shape was recorded again for the contact angle measurement.

Static Pressure Test under High Pressure. A sample was immersed in water inside a pressure chamber with the testing surface facing down. After a 10 μL air bubble was introduced to the surface through a needle, the system was sealed and pressurized to 0.5 MPa. The pressure was monitored with a high precision pressure gauge. The image of the air bubble during this process was recorded by a camera.

RESULTS AND DISCUSSION

The preparation of polymer nanotube arrays has been reported previously.[21,22] In this paper, PMMA nanotube arrays with a diameter (D) of 100 nm, wall thickness (T) of 10 nm and average groove width (P) of 50 nm were prepared. SEM images of the sample are shown in Figure 2. The surface was modified

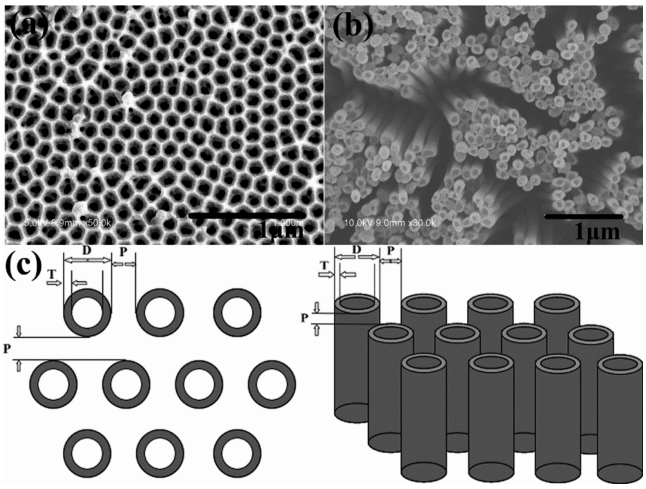

Figure 2. SEM images of (a) the AAO template, (b) the PMMA nanotube array, and (c) the structure model of the PMMA nanotube array with the designed structure ($D \approx 100$ nm, $T \approx 10$ nm, and $P \approx 50$ nm).

with two silicon coupling agents: PFO, a very low surface energy modifier, and PDNS, a high surface energy modifier. Consequently, three different PMMA nanotube array surfaces were obtained: those with a PFO coating, bare PMMA, and those with a PDNS coating. The intrinsic contact angles (θ) of these three substrates were measured on the corresponding smooth surfaces, which were prepared by modifying the smooth PMMA surfaces with the PFO and PDNS solutions in the same way used for the preparation of the superhydrophobic surfaces. The contact angles of these nanotube array surfaces were also detected and are compared in Table 1, where the corresponding slide angles (SA) are also listed.

Table 1. Results of the Water Contact Angle and Slide Angle Tests of the Smooth and Nanotube Array Surfaces

	smooth surface			nanotube array		
	PFO	PMMA	PDNS	PFO	PMMA	PDNS
CA (deg)	118	79	30	168	166	155
SA (deg)	15	60	>90	>1	3.5	12
f	1	1	1	0.041	0.025	0.05

The nanotube array surface will create complex wetting behavior, as indicated in Figure 3. For a water droplet placed on the surface, the wetting behaviors inside and outside the nanotube will differ. An additional pressure will build up inside the tube due to the formation of the closed space. This additional pressure will act against the external pressure, making this superhydrophobic surface very sticky to a water droplet.[22] In this work, under external impact, the water droplets were mainly forced into the intertube grooves, while very few water droplets were directed into the interiors of the tubes because the pressure inside the tubes counteracted the

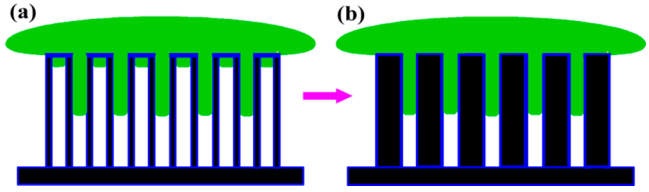

Figure 3. Comparison of the wetting behavior of (a) the nanotube array and (b) the pillar array surfaces. Water easily filled the grooves between the nanotubes and the pillars. The hole in the nanotube is only slightly filled with water because the increase in internal pressure prevents water from entering the tubes.

external pressure. This action caused the tubes to behave as pillars. Therefore, we can simplify the discussion by using a pillar array model to represent the nanotube array structure.

Table 1 shows that all three nanotube array surfaces display superhydrophobicity, indicating that the surfaces were at the Cassie–Baxter state with air trapped inside and between the nanotubes. The superhydrophobicity was nearly uncorrelated with the intrinsic water contact angle of the materials; i.e., a superhydrophobic surface can be constructed on low-energy and high-energy materials. The liquid-solid area fractions (f) of the three surfaces (PFO, PMMA, and PNDS) can be calculated from their corresponding θ' and θ values based on the Cassie–Baxter equation (eq 1), which gave fractions of 0.041, 0.025, and 0.05, respectively. These values are all much lower than the fraction of the solid area on top of the nanotube array, which was 0.145 (calculated from the structure model displayed in Figure 2c). This difference indicates that less than 35% of the nanotubes contacted the water droplet. This phenomenon is understandable based on the SEM images of the nanotube array (Figure 2), which showed that the nanotubes were not all the same height. The taller nanotubes were able to contact the water droplet. This result also indicates that approximately 35% of the nanotubes in the array were already sufficient to support the water droplet. Surprisingly, this fraction was similar to that for the highly hydrophilic substrate with the PDNS coating. This phenomenon can be understood only when the maximum pressure (p^{max}) of the surface is considered, which will be discussed in the following section.

Herminghaus proposed that a superhydrophobic surface can theoretically be constructed on materials with intrinsic contact angles lower than 90°. Later, this type of surface was experimentally achieved on high-energy materials such as poly(vinyl alcohol) (PVA).[23] However, this state can be realized only when the surface is maintained in the Cassie–Baxter mode. The stability of a rough surface maintained in the Cassie–Baxter mode can be determined from the maximum pressure (p^{max}) given by eq 3, which is derived from the circular pillar array model.[15] The water-pillar contact for a hydrophobic substrate is illustrated in Fig 4a according to this model. The water droplet can be held on the surface in the Cassie–Baxter mode due to the positive p^{max} value calculated from eq 3. However, if this pillar array is constructed from a hydrophilic material (i.e., $\theta < 90°$), eq 3 gives a negative value for p^{max}. This value means that the pressure will pull the water droplet into the grooves between the pillars to transition the surface from the Cassie–Baxter mode to the Wenzel mode. This condition indicates that a surface in the Cassie–Baxter mode is not stable or is only metastable. This analysis cannot explain the observation in our work that a contact angle as high as 155°

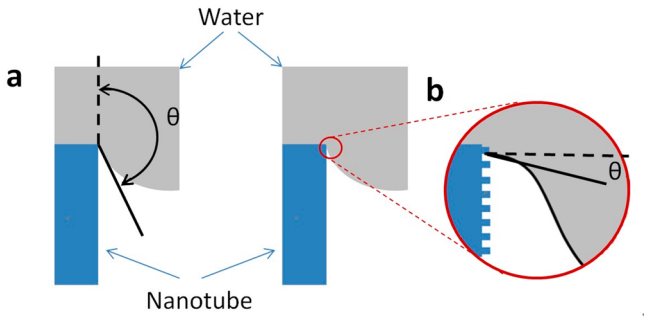

Figure 4. Illustration of water on the top of a circular pillar with an intrinsic contact angle (θ) (a) larger or (b) smaller than 90°. The nanometer-scale sub-pillar structure is also displayed as an inset in b for creating a positive p^{max}, as described by eq 5, to support a water droplet.

was achievable on the hydrophilic PDNS-coated nanotube array surface.

To understand this phenomenon, we must re-examine the surface structure of the nanotube at the nanometer scale. Polymer surfaces are usually rough at the nanometer scale. To simplify the discussion, we use a sub-pillar array structure to represent the roughness of the nanotube surface, as displayed in Figure 4b, where the outer wall of the nanotube is modified by an array of sub-pillars. The behavior of a water droplet on top of this binary structure will be similar to that of a water droplet on top of pillars with a nail-head structure, as demonstrated in the literature.[15] A positive p^{max} in eq 5 will be created on the interface to maintain the surface in the Cassie–Baxter mode. On the basis of this structure model, any rough surface structure with part of the surface area perpendicular to the nanotube wall will act as the nail-head structure to create a positive pressure to support the water droplet, even for θ values much lower than 90°. Equation 5 indicates that p^{max} is still correlated with the hydrophobicity of the substrate, with the intrinsic contact angle approaching 90°. A higher pressure will be created to support the water droplet, and therefore its Cassie–Baxter mode will be more stable. For example, the p^{max} on a PMMA surface is calculated to be approximately one-fold higher than the p^{max} on a PNDS surface. Additional increases in the hydrophobicity of the substrate that push θ beyond 90° will cause the regime to obey eq 3, where the resulting p^{max} value becomes more sensitive to the nanotube array structure. The variation in p^{max} with the basic parameters of the nanotube array D and P is displayed in Figure 5. The p^{max} value rapidly increases with decreasing groove width. When this value becomes lower than 15 μm, a p^{max} value larger than 10 kPa can be expected on the PFO substrate. This pressure is close to the heavy rain drop pressure,[24] indicating that a very stable superhydrophobicity can be expected on the PFO surface.

The p^{max} value acts as an energy barrier for the surface transition from the Cassie–Baxter mode to the Wenzel mode. Therefore, this transition only occurs at an external pressure equal to or larger than p^{max}. To verify this condition, we examined the superhydrophobic stabilities of these three surfaces by applying external pressures to the surfaces. Here, both the impact pressure and the static pressure were tested. For the impact pressure test, a 10 μL water droplet was released from different heights (h) above the surface to vary the impact pressure. The impact process from the droplet approaching the surface until reaching equilibrium was recorded using a high-speed camera. The data were analyzed, and the results are

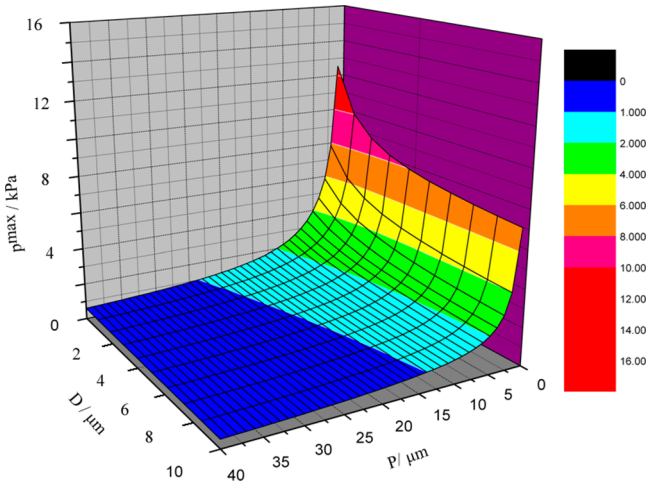

Figure 5. 3D illustration of eq 3, showing changes in the p^{max} value with changing parameters of the nanotube array (D and P), with D/T fixed at 100/10 for the PFO surface with θ' = 168°, indicating a high sensitivity of the p^{max} value to decreases in the groove width (D).

shown in Figure 6. The droplet can bounce a few cycles before an equilibrium contact angle (ECA) is reached on PFO and

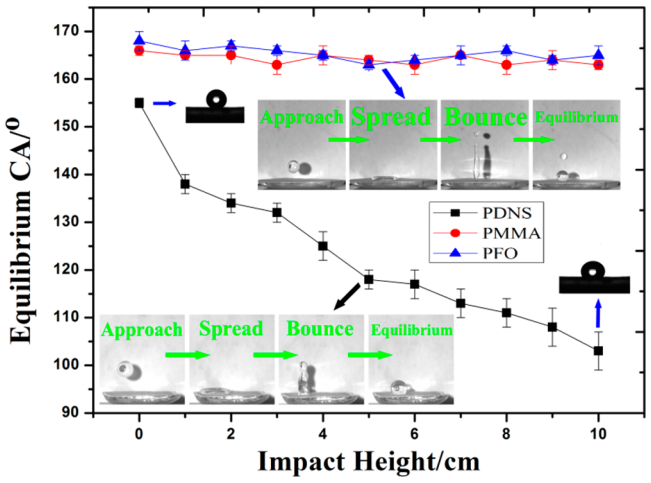

Figure 6. Equilibrium contact angle of a droplet released from different heights. The images show the impact processes of the droplet on the PFO/PMMA (inset, upper) and PDNS surfaces (inset, bottom).

PMMA. In contrast, the droplet only had several spreading and contracting cycles without any bouncing before equilibrium on the PDNS surface. The bounce number is displayed in Figure 7. The droplet on the PFO surface had the highest bounce number, followed by the PMMA and then the PDNS surfaces. Thus, the PFO surface has much higher superhydrophobicity with lower energy dissipation because of its lower surface friction.

Figure 6 also shows that the ECA is almost the same as the static contact angle (SCA) on both the PFO and PMMA surfaces for all of the tested impact heights from 0 to 10 cm. This similarity indicates highly stable superhydrophobicity. However, on the PDNS surface, the ECA decreased quickly with the impact height from 155° at h = 0 cm to 108° at h = 10 cm. This result indicates that the impact pressure does not overcome the maximum pressure (p^{max}) on the PFO and

dx.doi.org/10.1021/am500261c | ACS Appl. Mater. Interfaces 2014, 6, 8073–8079

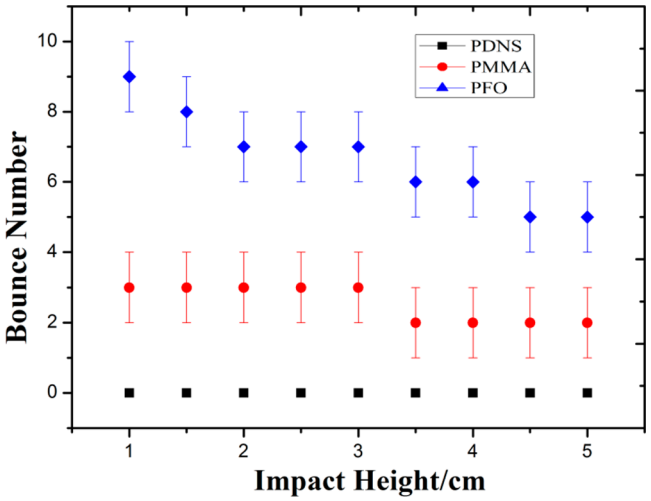

Figure 7. Bounce number of a droplet on the PFO, PMMA, and PDNS surfaces.

PMMA surfaces; therefore, no Cassie–Baxter mode to Wenzel mode transition occurred. This transition partially occurred on the PDNS surface, with the transition level increasing with impact pressure.

The impact pressure can be estimated from the impact height (h) of the droplet. Taking the volume of the water droplet, V = 10 μL = 1×10^{-8} m^3, we can calculate its mass, $m = 1 \times 10^{-5}$ kg, and diameter, $d = 2.68 \times 10^{-3}$ m. The energy of a water droplet when it reaches the surface depends on the impact height (h) and can be calculated from

$$E = mgh \tag{6}$$

where g is the gravity acceleration. On the basis of the assumption that the energy was completely dissipated during the impact and that the impact was completed from when the front of the water droplet touched the surface until the whole droplet reached the surface, we can take the diameter of the droplet (d) as the impact distance, and the average impact force during this process can be expressed as

$$F = \frac{E}{d} = \frac{mgh}{d} \tag{7}$$

Then, the impact pressure can be expressed as

$$p = \frac{F}{S} = \frac{F}{\pi\left(\frac{d}{2}\right)^2} = \frac{4mgh}{\pi d^3} \tag{8}$$

where S is the impact area, and the projected area of the droplet was taken for this value. From this equation, we can calculate the impact pressure of a 10 μL water droplet from a height of 10 cm as being 560 Pa. This equation indicates that the impact pressure increases linearly with the impact height. The impact testing result in Figire 6 shows that an increasing fraction of grooves is occupied by water as the impact pressure on the hydrophilic PDNS surface increases. Because the tops of the nanotubes on the surface are at different levels, more nanotubes will come into contact with the droplet as the impact pressure increase. Equation 5 indicates that the maximum pressure ($p^{max} = \gamma L \sin\theta/A$) increases with the ratio of L/A, where A is the projected water–air interface area and L is the sum of the perimeter of the pillars at the water/pillar boundary. With more nanotubes contacting water, the value of A will decrease, and L will increase, leading to an increase in the p^{max} value. The results of the impact test on PDNS confirmed that the hydrophilic nanotube array surface only partially lost its superhydrophobicity under dynamic impact because of the partial transition from the Cassie–Baxter mode to the Wenzel mode (Figure 6). The extent of the transition was determined by eq 5.

The static pressure test was conducted on the PDNS surface, as illustrated in Figure 8. A droplet (10 μL) of water was

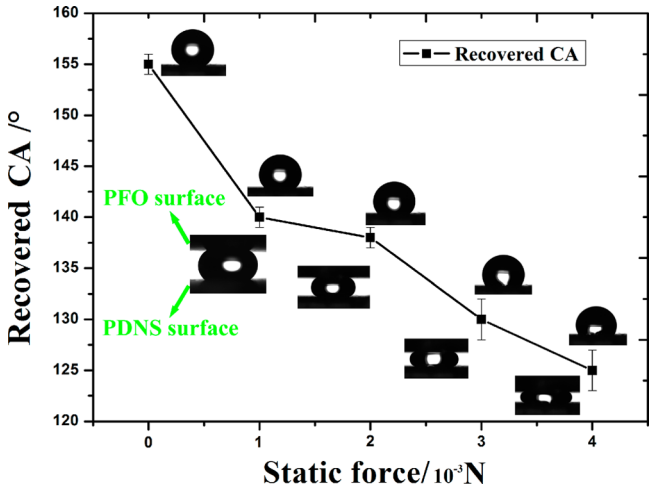

Figure 8. Variation in the recovered contact angles on the PDNS surface with the applied static force. The images of the water droplet during compression and after the force was removed are displayed as insets.

transferred to the top of the PDNS surface, and then a PFO plate was place on top of the water droplet with the PFO surface facing the droplet. Forces ranging from 0 to 0.004N were applied to the PFO plate. Because of the much higher superhydrophobicity of the PFO surface, the applied static pressure only induced the Cassie–Baxter mode to Wenzel mode transition on the PDNS surface, not on the PFO surface. After the static force and the top PFO plate were removed, the restored contact angle of the PDNS surface was recorded, and the result is displayed in Figure 8. The recovered contact angle decreased from 155° to 125° as the static force increased from 0 to 0.004N. To estimate the static pressure applied to the water/substrate interface, we assumed the contact area to be equal to the projected area of the water droplet, giving a pressure of 695 Pa when a 0.004Nforce was applied. This pressure was at the same level previously used for the dynamic impact pressure test, and similar recovered contact angles were observed for the dynamic impact and the static pressure tests (Figures 6 and 8).

The wetting state transition of these three surfaces under an extremely high pressure was also tested with the process described in Figure 9a–c, where the sample was immersed in water with the nanotube array surface facing down. When an air bubble was introduced onto the surface, as indicated in Figure 9d, because of the superhydrophobic property, a flat air layer was formed on the PFO surface, whereas an adsorbed air bubble with an almost flat water/air interface formed on the PMMA surface. The curvature of the interface slightly increased on the PDNS surface. This behavior is consistent with the water contact angles on the surfaces listed in Table 1. Then, the entire system was pressurized to 0.5 MPa, or ~5 atm, in a

dx.doi.org/10.1021/am500261c | ACS Appl. Mater. Interfaces 2014, 6, 8073–8079

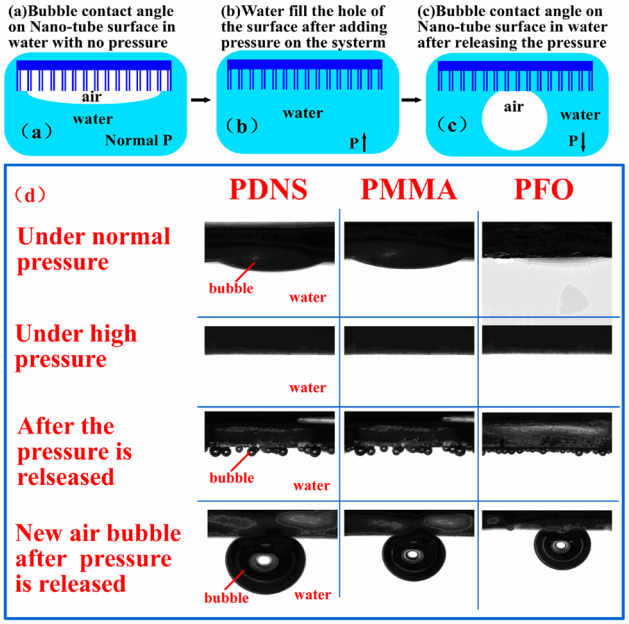

Figure 9. Illustration of an air bubble on a superhydrophobic surface (a) under atmospheric pressure, (b) under high pressure, and (c) after the high pressure was released. (d)Optical images of an air bubble on the PFO, PMMA and PDNS surfaces under atmospheric pressure, a high pressure of 0.5 MPa and after the high pressure was released.

pressure chamber. Under this external pressure, the volume of the air bubble on the surface and inside the grooves was reduced approximately 5-fold. The solubility of air in water will increase significantly under this high pressure according to Henry's law. The combination of these two factors results in the air bubble almost disappearing within the water-filled grooves and water-covered surface, as indicated in Figure 9b. This process converted the surface to the Wenzel state. When the pressure was reduced, the compressed air formed many tiny gas bubbles, partly from the compressed air and the air dissolved in water under high pressure. The three surfaces were retested by adding an air bubble to prove that the surface remained in the Wenzel state (Figure 9d). This result indicates that the wetting state transition of a hydrophobic surface from the Cassie–Baxter mode to the Wenzel mode is irreversible. Once this transition occurs, the Cassie–Baxter state of a hydrophobic surface cannot be easily recovered. Therefore, we conclude that the best approach to maintain superhydrophobicity is to increase the maximum pressure, p^{max}, of the surface beyond the external pressure applied to the surface, such as the impact pressure from raindrops. Increasing the contact angle of the material and the density of the nano-/microstructures are efficient ways to increase the maximum pressure.

CONCLUSION

We modified the PMMA nanotube array surface with different coupling agents to obtain three samples with intrinsic CAs ranging from 30 to 117°. All three surfaces showed superhydrophobic properties (CA > 150°), with a very small liquid-solid area fraction (f). These results confirmed that a small f value is important for superhydrophobicity, as proposed by the Cassie–Baxter equation. The energy barrier for the transition of the surface wetting state from the Cassie–Baxter mode to the Wenzel mode can be represented by the maximum pressure, p^{max}. This study revealed that p^{max} depends on the surface energy and the nanotube structure of the substrate as well as the nanometer-scale geometry of the nanotube surface structures. We showed that superhydrophobicity could be created on both low-energy surfaces and high-energy surfaces. The superhydrophobic stability of the low-energy surfaces, such as PFO and PMMA, was very high and could be easily maintained under low to medium testing pressures. However, the superhydrophobic stability of a high-energy material is much lower. For example, the water contact angle of the high-energy PDNS surface gradually decreased from 155 to approximately 120° as the external pressure increased from 0 to 695 Pa.

ASSOCIATED CONTENT

Supporting Information

The XPS spectra of the original sample modified by PFO and PDNS. F, N, C, O, and Si appeared in the spectra of the corresponding structures. The presence of these elements confirmed that the PFO and PDNS thin layers were successfully coated on the structure. The energy spectra of the carbon atom in different chemical environments indicated that the PFO and PDNS thin layers were successfully coated on the structure, respectively. These materials are available free of charge via the internet at http://pubs.acs.org.

AUTHOR INFORMATION

Corresponding Author

*E-mail: njuwqj@gmail.com.

Notes

The authors declare no competing financial interest.

ACKNOWLEDGMENTS

This work was supported by the Program for Changjiang Scholars and Innovative Research Team in University (PCSIRT) and the Key Laboratory of High Performance Polymer Materials & Technology, Ministry of Education of P. R. China. The authors are grateful to the National Defense Basic Scientific Research Program of China (Contract A0320132009) for supporting this work.

REFERENCES

(1) Lafuma, A.; Quere, D. Superhydrophobic States. *Nat. Mater.* **2003**, *2*, 457–460.
(2) Kwon, Y.; Patankar, N.; Choi, J.; Lee, J. Design of Surface Hierarchy for Extreme Hydrophobicity. *Langmuir* **2009**, *25*, 6129–6136.
(3) Guo, P.; Zheng, Y.; Wen, M.; Song, C.; Lin, Y.; Jiang, L. Icephobic/Anti-icing Properties of Micro/Nanostructured Surfaces. *Adv. Mater.* **2012**, *24*, 2642–2648.
(4) Zhang, W.; Yu, Z.; Chen, Z.; Li, M. Preparation of Superhydrophobic Cu/Ni Coating with Micro-nano Hierarchical Structure. *Mater. Lett.* **2012**, *67*, 327–330.
(5) Liu, W.; Luo, Y.; Sun, L.; Wu, R.; Jiang, H.; Liu, Y. Fabrication of the Superhydrophobic Surface on Aluminum Alloy by Anodizing and Polymeric Coating. *Appl. Surf. Sci.* **2013**, *264*, 872–878.
(6) Wang, Y.; Xue, J.; Wang, Q.; Chen, Q.; Ding, J. Verification of Icephobic/Anti-icing Properties of a Superhydrophobic Surface. *ACS Appl. Mater. Interfaces* **2013**, *5*, 3370–3381.
(7) Xiao, R.; Chu, K.-H.; Wang, E. N. Multilayer Liquid Spreading on Superhydrophilic Nanostructured Surfaces. *Appl. Phys. Lett.* **2009**, *94*, 193104.
(8) Fan, J.; Zhao, Y. Nanocarpet Effect Induced Superhydrophobicity. *Langmuir* **2010**, *26*, 8245–8250.

(9) Lipomi, D. J.; Kats, M. A.; Kim, P.; Kang, S. H.; Aizenberg, J.; Capasso, F.; Whitesides, G. M. Fabrication and Replication of Arrays of Single- or Multicomponent Nanostructures by Replica Molding and Mechanical Sectioning. *ACS Nano* **2010**, *4*, 4017−4026.
(10) Mishchenko, L.; Hatton, B.; Bahadur, V.; Taylor, J. A.; Krupenkin, T.; Aizenberg, J. Design of Ice-free Nanostructured Surfaces Based on Repulsion of Impacting Water Droplets. *ACS Nano* **2010**, *4*, 7699−7707.
(11) Cao, B.-Y.; Li, Y.-W.; Dong, R.-Y.; Kong, J.; Chen, H.; Xu, Y.; Yung, K.L. Superhydrophobicity of Self-Organized Surfaces of Polymer Nanowire Arrays Fabricated by a Nano-Injection Moulding Technique. *J. Therm. Sci. Technol.* **2011**, *6*, 204−209.
(12) Jung, Y. C.; Bhushan, B. Wetting Transition of Water Droplets on Superhydrophobic Patterned Surfaces. *Scr. Mater.* **2007**, *57*, 1057−1060.
(13) Patankar, N. A. Transition between Superhydrophobic States on Rough Surfaces. *Langmuir* **2004**, *20*, 7097−7102.
(14) Jopp, J.; Grull, H.; Yerushalmi-Rozen, R. Wetting Behavior of Water Droplets on Hydrophobic Microtextures of Comparable Size. *Langmuir* **2004**, *20*, 10015−10019.
(15) Lobaton, E. J.; Salamon, T. R. Computation of Constant Mean Curvature Surfaces: Application to the Gas-liquid Interface of a Pressurized Fluid on a Superhydrophobic Surface. *J. Colloid Interface Sci.* **2007**, *314*, 184−198.
(16) Gao, L.; McCarthy, T. J. How Wenzel and Cassie Were Wrong. *Langmuir* **2007**, *23*, 3762−3765.
(17) Koishi, T.; Yasuoka, K.; Fujikawa, S.; Ebisuzaki, T.; Zeng, X. C. Coexistence and Transition Between Cassie and Wenzel State on Pillared Hydrophobic Surface. *Proc. Natl. Acad. Sci. U.S.A.* **2009**, *106*, 8435−40.
(18) Bucher, T. M.; Emami, B.; Tafreshi, H. V.; Gad-el-Hak, M.; Tepper, G. C. Modeling Resistance of Nanofibrous Superhydrophobic Coatings to Hydrostatic Pressures: The Role of Microstructure. *Phys. Fluids* **2012**, *24*, 022109.
(19) Kim, T. J.; Hidrovo, C. Pressure and Partial Wetting Effects on Superhydrophobic Friction Reduction in Microchannel Flow. *Phys. Fluids* **2012**, *24*, 112003.
(20) Samaha, M. A.; Vahedi Tafreshi, H.; Gad-el-Hak, M. Sustainability of Superhydrophobicity under Pressure. *Phys. Fluids* **2012**, *24*, 112103.
(21) Martin, J.; Mijangos, C. Tailored Polymer-based Nanofibers and Nanotubes by means of Different Infiltration Methods into Alumina Nanopores. *Langmuir* **2009**, *25*, 1181−1187.
(22) Jin, M. H.; Feng, X. J.; Feng, L.; Sun, T. L.; Zhai, J.; Li, T. J.; Jiang, L. Superhydrophobic Aligned Polystyrene Nanotube Films with High Adhesive Force. *Adv. Mater.* **2005**, *17*, 1977.
(23) Feng, L.; Song, Y.; Zhai, J.; Liu, B.; Xu, J.; Jiang, L.; Zhu, D. Creation of a Superhydrophobic Surface from an Amphiphilic Polymer. *Angew. Chem., Int. Ed.* **2003**, *42*, 800−802.
(24) Bormashenko, E. Wetting Transitions on Biomimetic Surfaces. *Philos. Trans. R. Soc., A* **2010**, *368*, 4695−4711.